CHEMISTRY OF MATERIALS

ARTICLE

pubs.acs.org/cm

Can Vanadium Be Substituted into $LiFePO_4$?

Fredrick Omenya,[†] Natasha A. Chernova,[‡] Shailesh Upreti,[‡] Peter Y. Zavalij,[§] Kyung-Wan Nam,[∥] Xiao-Qing Yang,[∥] and M. Stanley Whittingham*[,†,‡]

[†]Department of Chemistry, State University of New York at Binghamton, Binghamton, New York 13902-6000, United States

[‡]Materials Science and Engineering Program, State University of New York at Binghamton, Binghamton, New York 13902-6000, United States

[§]Department of Chemistry and Biochemistry, University of Maryland, College Park, Maryland 20742, United States

[∥]Chemistry Department, Brookhaven National Laboratory, Upton, New York 11973, United States

ABSTRACT: Vanadium is shown to substitute for iron in the olivine $LiFePO_4$ up to at least 10 mol %, when the synthesis is carried out at 550 °C. In the solid solution $LiFe_{1-3y/2}V_yPO_4$, the *a* and *b* lattice parameters and cell volume decrease with increasing vanadium content, while the *c* lattice parameter increases slightly. However, when the synthesis is performed at 650 °C, a NASICON phase, $Li_3V_2(PO_4)_3$, is also formed, showing that solid solution is a function of the synthesis temperature. X-ray absorption near-edge structure indicates vanadium is in the 3+ oxidation state and in an octahedral environment. Magnetic studies reveal a shift of the antiferromagnetic ordering transition toward lower temperatures with increasing vanadium substitution, confirming solid solution formation. The addition of vanadium enhances the electrochemical performance of the materials especially at high current densities.

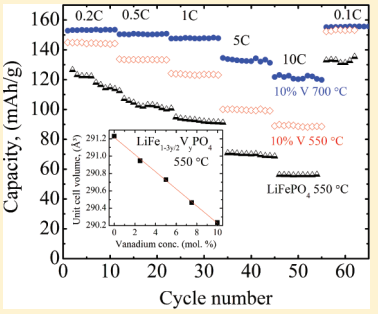

KEYWORDS: olivine phosphates, vanadium substitution, electrochemical properties

INTRODUCTION

$LiFePO_4$ has been extensively studied as an electrode for lithium batteries, as it possesses good thermal stability, is potentially low cost, and is environmentally benign.[1] However, it suffers from a low electronic conductivity, and Li removal and insertion appear to be slow for large particles. The use of nanosize particles allows for fast lithium reaction,[2,3] and to improve the electronic conductivity, two major approaches have been proposed: (1) coating the particles with a conductive film such as conductive carbon[4] and/or (2) aliovalent doping. The report of an increased electronic conductivity of this material by about 8 orders of magnitude when doped at the ppm level[5] is almost certainly caused by the formation of a conductive coating of Fe_2P under the high-temperature reducing reaction conditions used.[6]

In the ordered olivine structure of $LiFePO_4$, the low-valent cation (Li) resides at the M1 site and the higher charged cation (Fe) resides at the M2 site. However, disorder is quite common. For example, when $LiFePO_4$ is hydrothermally synthesized at 120 °C, around 7% Fe is found on the Li site, but on increasing the temperature to 190 °C, less than 1% Fe disorder is observed. In addition, excess iron is also reportedly found in the structure and then resides on the Li site. Isovalent substitution is normal in nature, $Li(Mn,Fe)PO_4$, and many divalent cations can be substituted from 0 to 100%, including Mn, Co, Ni, and Mg, and others such as Zn^{2+} and Ca^{2+} can be partially substituted to lower levels.[7] Atomistic simulations show favorable energies for divalent ion substitution at the Fe site but speak against the possible substitution of supervalent ions on either the Fe or Li site.[8]

Vanadium is a particularly attractive element to consider for substitution in the olivine lattice, as it readily forms phosphates and exists over a wide range of oxidation states and in different polyhedra with oxygen, so it might substitute on the octahedral Fe site forming a VO_6 group or on the tetrahedral P site forming a VO_4^{3-} group. Although there have been several reports on vanadium substitution to improve the electrochemical performance of $LiFePO_4$,[9−13] there is much disagreement about its role varying from structure modification by substitution for Fe, P, or Li leading to enhanced Li or electron mobility, second phase formation, or formation of a conductive coating on the $LiFePO_4$. In these works, vanadium substitution at the Fe site was targeted; however, there is no consistency in the reported lattice parameters and vanadium location in the lattice. We reported earlier on the possible substitution on the P site[9] leading to the unit cell volume decrease. Hua et al.[10] and Ma et al[11] reported a linear decrease of the cell volume upon substitution up to 4 and 7 mol % vanadium, respectively, at a Fe site, while Sun et al.[12] observed cell volumes increase with 3 mol % substitution and Zhang et al.,[13] substituting up to 5% vanadium, observed irregular cell volume changes. Jin et al.[14] observed no cell volume change upon adding up to 10 mol % V to the 1:1:1 Li/Fe/P precursor ratio, concluded no vanadium substitution, and attributed enhanced electrochemical performance to the conductive V_2O_3 incorporated into the carbon coating. Aleees[15] also reported the formation

Received: June 15, 2011
Revised: September 22, 2011
Published: October 13, 2011

dx.doi.org/10.1021/cm2017032 | *Chem. Mater.* 2011, 23, 4733–4740

of a composite $LiFePO_4 \cdot zV_2O_3$, with no V substitution in the $LiFePO_4$ lattice but surprisingly showing a cell volume decrease to 288.9 Å. Zhao et al.[16] claimed that "both experimental and theoretical simulations show that vanadium does not enter into the $LiFePO_4$ crystal lattice", not even at the 1% substitution level, based on the X-ray absorption data analysis. The data on the vanadium oxidation state are also inconsistent: when the Fe site substitution is aimed, 3+,[12] between 3 and 4+,[13] and 4+ oxidation states are reported.[11] Manthiram even proposed that vanadium may be substituted into $LiFePO_4$ as V^{4+} in the vanadyl $(VO)^{2+}$ ion.[17] When V substitutes on the P site, it assumes V^{5+} in the tetrahedral $(VO_4)^{3-}$.[9]

The purpose of this study is to determine whether indeed vanadium can be substituted into the olivine lattice, which site it resides on, what is its oxidation state, and what is the impact on the electrochemical behavior. We have investigated substitution at Li, Fe, and P sites tailoring precursor's ratios for various vanadium oxidation states and charge compensation mechanisms. We have found that up to 10 mol % vanadium can be substituted at the Li site when the solid solution is formulated as $Li_{1-3x}V_x$-$FePO_4$ and at the Fe site forming $LiFe_{1-3y/2}V_yPO_4$, when the synthesis is performed at 550 °C. The attempts to intentionally substitute the P site were unsuccessful. In this paper, we focus on $LiFe_{1-3y/2}V_yPO_4$ series, where the highest vanadium solubility combined with the best electrochemical performance were achieved.

EXPERIMENTAL SECTION

The $LiFePO_4$ samples were synthesized by the solid-state reaction of Li_2CO_3, $FeC_2O_4 \cdot 2H_2O$, $NH_4H_2PO_4$, and NH_4VO_3. Stoichiometric amounts of the precursors for the $LiFe_{1-3y/2}V_yPO_4$ (y = 0, 0.025, 0.05, 0.075, 0.10, 0.20) series and for the $LiFe_{1-y}V_yPO_4$ (y = 0, 0.05, 0.07) series were mixed together. Carbon black (5 wt %) was added to the mixture, which was planetary ball-milled in acetone for 12 h. The acetone was evaporated and dried. The resulting precursors were preheated at 350 °C for 8 h before sintering at either 550 or 700 °C for 10 h in a 8.5% H_2/He atmosphere in a temperature-controlled tube furnace. We will refer to these series using the precursor compositions; the actual compositions and charge compensation mechanisms will be discussed later.

The phase composition and the crystal structure of the synthesized samples were determined by powder X-ray diffraction (XRD) using a Scintag XDS2000 θ-θ diffractometer equipped with a Ge(Li) solid state detector and Cu Kα sealed tube (λ = 1.541 78 Å). The data were collected in the range of 2θ = 10−80° with a step size of 0.02° while spinning the sample to minimize preferred orientation. High-resolution synchrotron powder XRD data were collected using beamline 11-BM at the Advanced Photon Source (APS), Argonne National Laboratory, with an average wavelength of 0.413 612 Å. XRD powder Rietveld refinement was performed to determine the lattice parameters and site occupancy for the synthesized samples using the GSAS/EXPGUI package.[18,19] X-ray absorption spectroscopy (XAS) experiments were carried out on the X23A2 beamline at the National Synchrotron Light Source at Brookhaven National Laboratory, a bending magnet beamline equipped with Si(311) monochromator. The Fe K-edge spectra and V K-edge spectra of reference samples, $Li_3V_2(PO_4)_3$, V_2O_5, VO_2, and VCl_2, were collected in transmission mode. The V K-edge spectra of the substituted samples were measured in the fluorescence mode using a 4-element Si drift detector for energy dispersive measurements of dilute systems. Athena software was used for the XAS data analysis.[20] The morphology and particle sizes were obtained by high-resolution scanning electron microscopy (SEM), ZeissSupra-55 field emission scanning electron microscope, operating at 10 kV. The superconducting quantum interference device (SQUID) magnetometer (Quantum Design MPMS XL-5) was used to measure the dc magnetic susceptibility (χ) of the samples from 350 to 2 K in a 1000 Oe magnetic field.

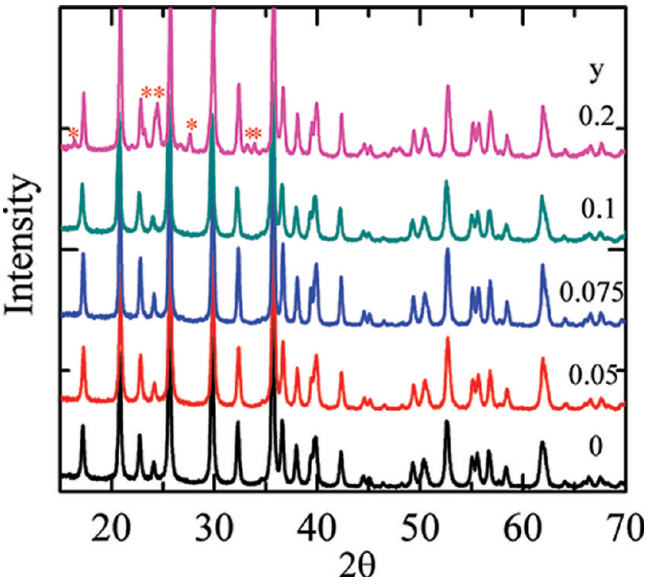

Figure 1. X-ray diffraction patterns for $LiFe_{1-3/2y}V_yPO_4$ (y = 0, 0.05, 0.075. 0.10, 0.20) synthesized at 550 °C; the asterisks indicate the peaks of the $Li_3V_2(PO_4)_3$ phase formed at y = 0.20.

The cathode materials for the electrochemical tests were prepared by mixing 80% active material, 12% carbon black (total amount of carbon in the electrode), and 8% polyvinylidene fluoride (PVDF) with 1-methyl-2-pyrrolidinone solvent. The slurry formed was then cast onto an Al foil current collector before drying. The dried electrodes, of area 1.2 cm^2, containing 3−5 mg of active material were placed in 2325-type coin cells in a He-filled glovebox with pure lithium foil (Aldrich, thickness 23 μm) as the counter and reference electrodes and Celgard 2400 as the separator. $LiPF_6$ (1 M) in a 1:1 volume ratio of ethylene carbonate (EC) and dimethyl carbonate (DMC) (LP30 from EMIndustries) was used as the electrolyte. The cells were tested using a VMP2 multichannel potentiostat (Biologic). The galvanostatic charge and discharge experiments were performed at current densities corresponding to 0.1, 0.2, 0.5, 1, and 10C rates (1C corresponds to 160 mAh/g) over a 2.0−4.3 V voltage range. The cyclic voltammetry (CV) test was done at a slow scanning rate of 0.02 mV/s in a voltage range of 2.5−4.3 V vs Li^+/Li.

RESULTS AND DISCUSSION

The X-ray diffraction patterns, shown in Figure 1, of $LiFe_{1-3/2y}V_yPO_4$ (y = 0.025, 0.05, 0.075. 0.10, 0.20) series synthesized at 550 °C show a single orthorhombic structure with no observable impurity peaks for $0 \le y \le 0.1$. For y = 0.20, a second phase of $Li_3V_2(PO_4)_3$ is observed. The unit cell parameters, determined by Rietveld refinement and shown in Figure 2 and Table 1, obey Vegard's law, with the a and b lattice parameters and the cell volume decreasing linearly with the increase in the vanadium concentration and the c parameter showing a very small increase. This indicates that vanadium forms a solid solution with the iron in the $LiFePO_4$ lattice.

High-resolution synchrotron XRD patterns of selected samples (y = 0.05, 0.1) confirmed the phase purity, with no impurity peaks being detected (Figure 3). This data was used to refine the site occupancies to reveal the charge compensation mechanism. The refinement shows nearly full occupancy (98.5%) of the

dx.doi.org/10.1021/cm2017032 |Chem. Mater. 2011, 23, 4733–4740

Li site for both $y = 0.05$ and 0.1, meaning that no heavy ions, such as V or Fe, are present at the Li site. An attempt to force V to the Li site leads to strong *R*-factors increase, for example, structural *R*-factor $R(F^2)$ increases from 1.8 to 4.4 if 10% V is placed at Li site. Thus, Li site occupancy was fixed at 100% Li and the occupancy of the iron site was refined revealing vacancy formation. When the iron to vanadium ratio and occupancy were fixed as in the precursor compositions, $LiFe_{1-3/2y}V_y\square_{y/2}PO_4$ ($y = 0.05$ and 0.1), the *R*-factors increased slightly, $R(F^2) = 2.0$, so another refinement, constraining just the charge balance on the Fe site, was performed. It resulted in $LiFe_{0.943(1)}V_{0.038(1)}PO_4$ and $LiFe_{0.904(1)}V_{0.064(1)}PO_4$ compositions for $y = 0.05$ and 0.1, respectively, with $R(F^2)$ about 1.7. These formulas show just a bit less vanadium than in the initial reactant compositions. Taking into account the poor resolution between Fe and V in X-ray diffraction and only minor *R*-factor improvement upon V and Fe content refinement, we consider the Rietveld results consistent with the formulated compositions. The number of vacancies on the Fe site is consistent with vanadium being in the 3+ oxidation state. An attempt to fix the Fe site occupancy at 100% and refine the Li site occupancy gives 103% Li-site occupancy with a higher $R(F^2)$ of 1.9 and less reliable thermal displacement parameters. However, vacancy formation at both Fe and Li sites cannot be totally excluded based on the XRD data refinement due to poor resolution between the Li ion and vacancy.

When carbon is not used in the synthesis, a pure olivine phase is not achieved, indicating the key role of carbon in the reduction of the V^{5+} in the precursor and, probably, as a stabilizer of the reduced vanadium ion. Also, attempts to synthesize $LiFe_{1-y}V_yPO_4$ solid solutions, assuming V^{2+}, at the same conditions indicated much lower solubility level, and impurity peaks were observed at 7 mol % V substitution, which suggests that these

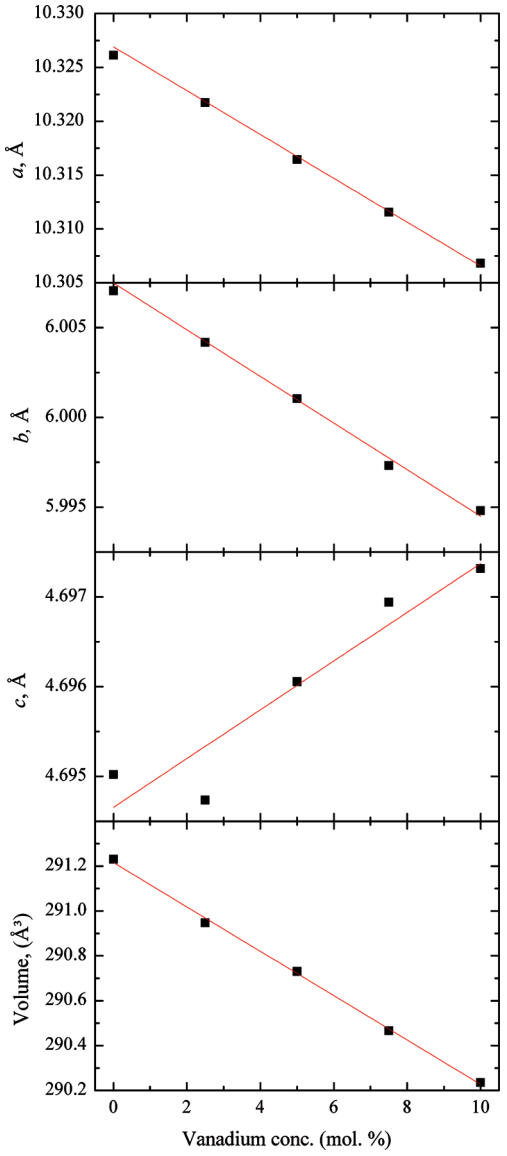

Figure 2. Lattice parameters and cell volume of $LiFe_{1-3/2y}V_yPO_4$ as a function of vanadium content.

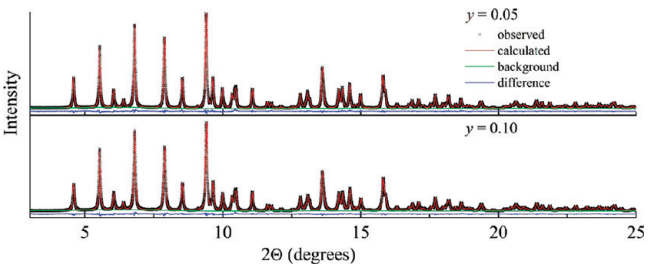

Figure 3. Rietveld refinement of high-resolution synchrotron X-ray diffraction data for $LiFe_{1-3/2y}V_yPO_4$ ($y = 0.05$ and 0.10) synthesized at 550 °C.

Table 1. Lattice Parameters of $LiFe_{1-3/2y}V_yPO_4$

targeted composition	synthesis temperature (°C)	*a* (Å)	*b* (Å)	*c* (Å)	*V* (Å^3)	R_p
$LiFePO_4$	550	10.3261(2)	6.0071(1)	4.6950(1)	291.230	4.29
	700	10.3282(1)	6.0085(1)	4.6942(1)	291.310	5.07
$LiFe_{0.9625}V_{0.025}PO_4$	550	10.3217(2)	6.0042(1)	4.6947(1)	290.947	4.19
$LiFe_{0.925}V_{0.05}PO_4$	550	10.3164(2)	6.0010(1)	4.6962(1)	290.730	4.07
	700	10.3144(1)	6.0021(1)	4.6970(2)	290.782	4.43
$LiFe_{0.8875}V_{0.075}PO_4$	550	10.3115(2)	5.9973(1)	4.6969(1)	290.466	4.21
$LiFe_{0.85}V_{0.1}PO_4$	550	10.3068(3)	5.9948(1	4.6973(1)	290.235	4.09
	700	10.3093(3)	5.9991(1)	4.6979(1)	290.549	5.07
$LiFe_{0.85}V_{0.1}PO_4$[a]	550 and 700	10.318 7(1)	6.001 2(1)	4.693 6(1)	290.651	6.42
$LiFe_{0.925}V_{0.05}PO_4$[b]	550	10.313 68(4)	5.999 67(3)	4.694 61(2)	290.497	3.56
$LiFe_{0.85}V_{0.1}PO_4$[b]	550	10.304 21(5)	5.993 50(3)	4.696 00(3)	290.017	3.24

[a] 550 °C sample heat treated at 700 °C for 10 h. [b] High-resolution synchrotron X-ray diffraction data with occupancy refinement.

dx.doi.org/10.1021/cm2017032 |*Chem. Mater.* 2011, 23, 4733–4740

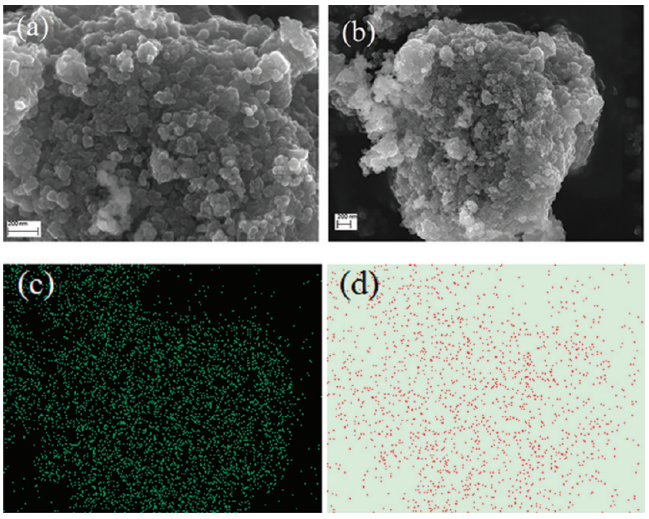

Figure 4. SEM images of (a) $LiFePO_4$ and (b) $LiFe_{0.925}V_{0.05}PO_4$ synthesized at 550 °C along with EDX mapping of (c) iron and (d) vanadium.

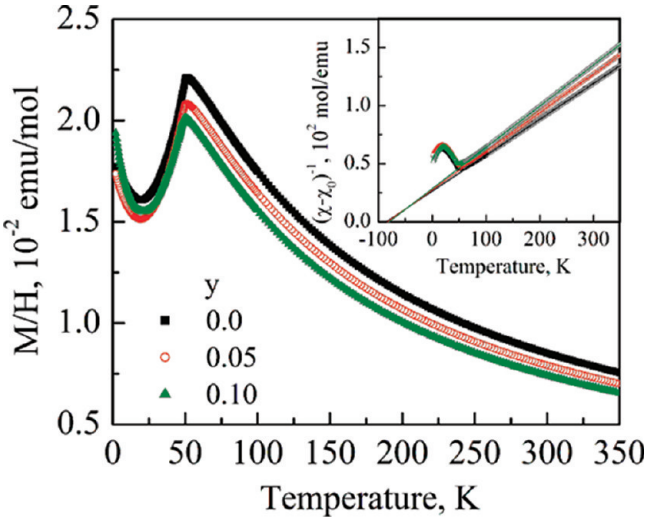

Figure 5. Temperature dependences of the magnetic susceptibility of $LiFe_{1-3y/2}V_yPO_4$ synthesized at 550 °C; inset shows inverse susceptibilities corrected for temperature-independent contribution and their fit to the Curie–Weiss law.

synthesis conditions and/or the geometry of the iron site in the $LiFePO_4$ crystal structure favor V^{3+} substitution. The results thus support the solid solution formula $LiFe_{1-3/2y}V_y\square_{y/2}PO_4$ rather than $LiFe_{1-y}V_yPO_4$ where all the sites are fully occupied; vacancies at the Fe site are clearly observed in the Rietveld refinement, however partial charge compensation by vacancies on the Li site cannot be excluded.

Figure 4a,b shows the SEM micrographs of pristine and $LiFe_{0.925}V_{0.05}PO_4$ samples. The particles are nearly spherical, nanosized with a narrow particle size distribution of about 40–50 nm. The particles agglomerate forming secondary particles, which are independent of substitution level. The elemental mapping in Figure 4c,d corresponding to the 5 mol % vanadium substituted sample micrograph confirms that vanadium is uniformly dispersed.

The magnetic properties were studied to confirm sample purity, transition metal oxidation states, and structural ordering, since magnetic properties are more sensitive to these issues than X-ray diffraction. The temperature dependence of the magnetic susceptibility of $LiFe_{1-3y/2}V_yPO_4$ (Figure 5) shows the expected paramagnetic behavior at high temperatures and antiferromagnetic ordering below 50 K; no additional magnetic transitions or increased magnetic susceptibility are found confirming the absence of magnetic impurities, such as Fe_3O_4, Fe_2P, V_2O_3, or vanadium phosphates. The Neel temperature, T_N, decreases with an increase of vanadium content meaning that vanadium is indeed substituted into the $LiFePO_4$ structure weakening the magnetic interactions between transition metal ions due to lower, as compared to Fe^{2+}, magnetic moment and the presence of vacancies at the Fe site. The Curie–Weiss law was used to fit the paramagnetic part of the dependences (inset in Figure 5) and to determine the Curie constant and Curie–Weiss temperatures (Table 2). With the increase of vanadium content, the absolute values of the Curie–Weiss temperature slightly decrease, which is consistent with weakening of the antiferromagnetic exchange on vanadium substitution, the effect already observed in T_N dependence on the vanadium content. The Curie constant also decreases with vanadium substitution, because the vanadium ions in either the 2+ or 3+ oxidation state have a lower number of unpaired

Table 2. Magnetic Parameters of $LiFe_{1-3y/2}V_yPO_4$ Series[a]

y	T_N, K	χ_0, emu/mol	Θ, K	C, emu K/mol	μ_{eff}^{exp}, μ_B	μ_{eff}^{theor}, μ_B
0	49.2	1.2×10^{-4}	−85.8	3.240	5.09	5.09
0.05	48.0	6.1×10^{-5}	−83.1	3.009	4.97	5.00
0.1	47.0	2.9×10^{-6}	−80.6	2.817	4.87	4.90

[a] T_N is determined as an inflection point of the $M(T)$ dependence; μ_{eff}^{exp} is determined using $\mu = [8C/(1 - y/2)]^{1/2}$; in calculations of μ_{eff}^{theor}, the magnetic moment of Fe^{2+} is assumed $5.09\mu_B$, as in $LiFePO_4$, since it is difficult to account for its orbital contribution; the magnetic moment of V^{3+} is assumed as spin-only $2.82\mu_B$.

electrons and, consequently, lower effective magnetic moment than Fe^{2+}. The average effective magnetic moment per transition ion, calculated assuming that iron has the same magnetic moment as in $LiFePO_4$ and vanadium in the 3+ oxidation state ($S = 1$, $\mu_{eff} = 2.82\mu_B$) as suggested by the series composition, agrees well with the experimentally observed values (Table 2).

X-ray absorption near edge structure (XANES) was used to further confirm the oxidation states and to investigate local environments of vanadium and iron in the compounds. XANES spectra of $LiFe_{1-3y/2}V_yPO_4$ ($y = 0.05$ and 0.1) at V K edge compared to those of vanadium 2+ to 5+ reference compounds (Figure 6) reveal that vanadium absorption edges appear at the same energy through the whole series and match with the absorption edge of $Li_3V_2(PO_4)_3$, thus, indicating a V^{3+} oxidation state. The pre-edge feature corresponding to a 1s to 3d transition has a double-peak structure and decreases in intensity with increasing vanadium content. This transition is possible due to the distortion of VO_6 octahedra, and the decrease in intensity indicates that VO_6 octahedra become of more regular geometry as more V is substituted in $LiFePO_4$. In addition, the weak V K-edge pre-edge intensities for the V substituted $LiFePO_4$ suggest the V atoms mostly reside in the octahedral site (M1 or M2) rather than the tetrahedral site (P site in the PO_4 unit). Considering the refinement results, X-ray absorption confirms

dx.doi.org/10.1021/cm2017032 |Chem. Mater. 2011, 23, 4733–4740

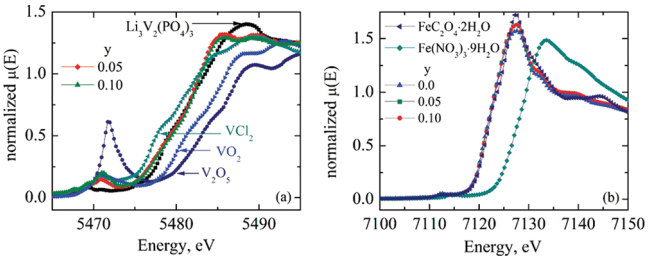

Figure 6. X-ray absorption near edge structure at (a) vanadium K-edge and (b) iron K-edge of $LiFe_{1-3y/2}V_yPO_4$ synthesized at 550 °C together with (a) VCl_2, $Li_3V_2(PO_4)_3$, VO_2, and V_2O_5 used as vanadium 2+, 3+, 4+, and 5+ standards, respectively; and (b) $FeC_2O_4 \cdot 2H_2O$ and $Fe(NO_3)_3 \cdot H_2O$ used as Fe^{2+} and Fe^{3+} standards.

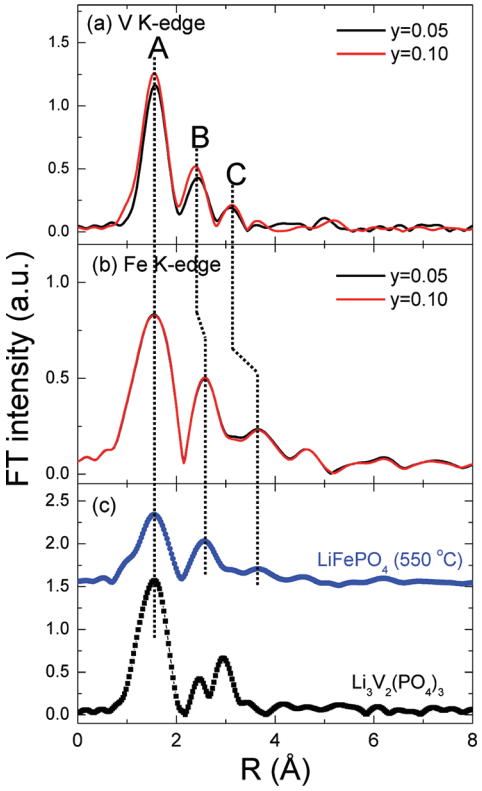

Figure 7. Magnitudes of Fourier transforms of the k^2-weighted EXAFS spectra at (a) V K-edge and (b) Fe K-edge of $LiFe_{1-3y/2}V_yPO_4$ ($y = 0.05$ and 0.1) synthesized at 550 °C in comparison with (c) those of $LiFePO_4$ synthesized at 550 °C at the Fe K edge and $Li_3V_2(PO_4)_3$ at the V K edge. The Fourier transform was not phase corrected so that the actual bond lengths may be ~0.2−0.4 Å longer.

V substitution of Fe atoms in the FeO_6 octahedra (M2 site) in the olivine structure. Fe K-edge spectra do not show any shift or change in the pre-edge intensity with vanadium substitution, meaning that the iron oxidation state remains 2+ and the local Fe environment is not affected much by the V substitution.

In order to investigate local structures around V and Fe in the compounds, magnitudes of Fourier transforms (FTs) of k^2 weighted extended X-ray absorption fine structure (EXAFS) spectra for $LiFe_{1-3y/2}V_yPO_4$ ($y = 0.05$ and 0.1) samples at V and Fe K edges are shown in Figure 7 in comparison with those of undoped $LiFePO_4$ synthesized at 550 °C at Fe K edge and

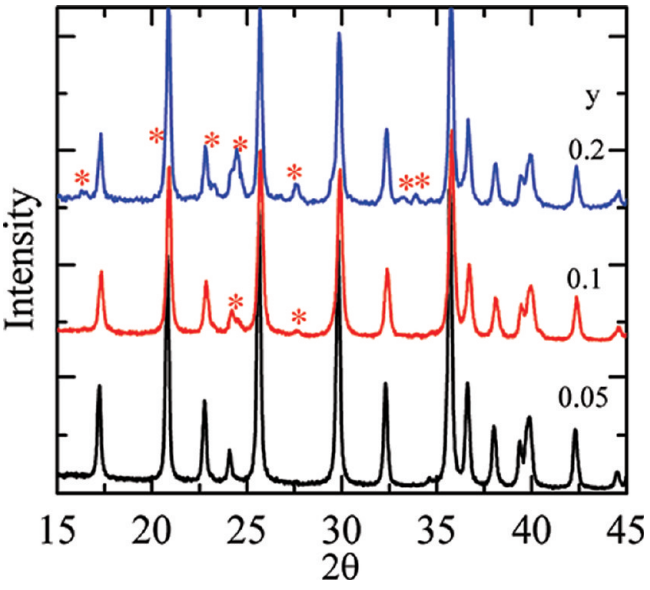

Figure 8. XRD patterns of $LiFe_{1-3/2y}V_yPO_4$ (y = 0.05, 0.1, 0.2) synthesized at 700 °C; the asterisks indicate $Li_3V_2(PO_4)_3$ peaks.

$Li_3V_2(PO_4)_3$ references at the V K edge. In all cases, FTs were done in a k-range from 3.0 to 10.0 $Å^{-1}$ with a Kaiser−Bessel window to obtain the magnitude plots of the EXAFS spectra in an R-space.

The FT features of the first three shells around the V atoms [A, B, and C in Figure 7a] are more analogous to the olivine $LiFePO_4$ structure than the NASICON $Li_3V_2(PO_3)_4$ structure in terms of the intensity variation. The local structure around Fe atoms in Figure 7b also shows typical features of the olivine structure. A, B, and C shells represent the six Fe(V)−O, five Fe(V)−P, and two Fe(V)−Fe/V interactions in the olivine structure, respectively. This result strongly suggests the vanadium substitution of the Fe (M2) site in the olivine structure. However, when compared to the local structure around Fe (Figure 7 (b)), shorter V−P (B shell) and V−Fe/V (C shell) bond lengths, and relatively stronger first V−O shell intensity are observed around V atoms (Figure 7a). This might be related to the local clustering of V, and further analysis is needed to obtain more detailed information about the local structure around V in the $LiFe_{1-3y/2}V_yPO_4$. Our X-ray absorption results contradict ref 16, where both XANES and EXAFS of $LiFe_{0.95}V_{0.05}PO_4$ and $LiFeP_{0.95}V_{0.05}O_4$ were found similar to that of $Li_3V_2(PO_4)_3$ and no vanadium substitution was claimed. Since no structural characterization beyond XAS is presented in ref 16, it is not possible to rationalize this discrepancy.

The role of synthesis temperature on vanadium substitution into $LiFePO_4$ was investigated by raising the sintering temperature from 550 to 700 °C. XRD patterns of the samples sintered at 700 °C show $Li_3V_2(PO_4)_3$ impurity peaks at 10 mol % substitution; the peaks increase in intensity with a further increase of vanadium content (Figure 8). At 5% substitution, no observable impurity phase is detected from lab XRD or high-resolution synchrotron XRD; however, the electrochemistry results to be discussed below show the presence of some amount of $Li_3V_2(PO_4)_3$. This has led us to a conclusion that at a higher temperature, 700 °C, some of the vanadium is ejected from the olivine structure forming a $Li_3V_2(PO_4)_3$ minor phase. Rietveld refinement of the 5 mol % substituted sample synthesized at

dx.doi.org/10.1021/cm2017032 |Chem. Mater. 2011, 23, 4733–4740

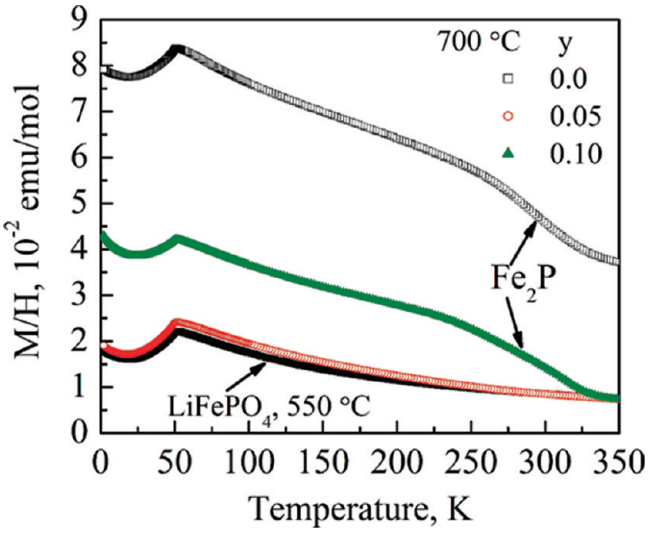

Figure 9. Temperature dependences of the magnetic susceptibility of $LiFe_{1-3y/2}V_yPO_4$ synthesized at 700 °C; temperature dependence for the 550 °C $LiFePO_4$ sample is given for comparison.

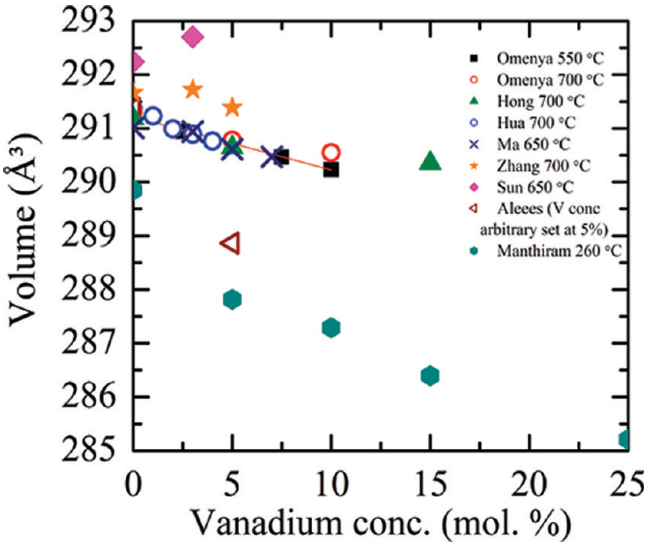

Figure 10. Unit cell volumes as a function of vanadium content in $LiFePO_4$ obtained in the present work (Omenya 550 and 700 °C) and available in the literature.

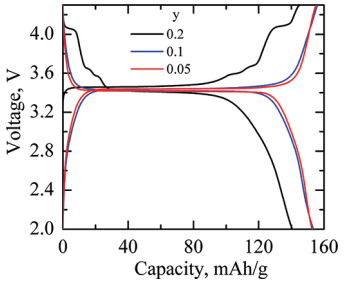

Figure 11. Galvanostatic charge−discharge curves measured at 0.1*C* (0.07 mA/cm^2) for $LiFe_{1-3/2y}V_yPO_4$ (y = 0.05, 0.1, 0.2) synthesized at 550 °C.

700 °C shows a slightly smaller unit cell dimension than the pristine one synthesized at the same temperature, supporting the hypothesis that not all the vanadium ions have been extruded from the structure (Table 1). This point was further confirmed by heat-treating a single-phase $LiFe_{0.85}V_{0.1}PO_4$ synthesized at 550 at 650 °C and 700 °C in He/H_2 mix for 10 h, giving olivine phase, $Li_3V_2(PO_4)_3$ and Fe_2P products. The cell volume of the resulting olivine phase is slightly smaller than that of unsubstituted $LiFePO_4$ but larger than of the single phase $LiFe_{0.85}V_{0.1}PO_4$ and corresponds roughly to 6 mol % vanadium substitution (Table 1). Magnetic studies of the samples synthesized at 700 °C reveal increased susceptibility in comparison to the samples synthesized at 550 °C (Figure 9). The major susceptibility increase occurs between 200 and 300 K, which is typical of $LiFePO_4$ samples with Fe_2P impurity undergoing ferromagnetic ordering at 215 K.[21] Fe_2P forms as a result of over-reduction at 700 °C; it is an electronically conductive impurity and beneficial for the electrochemical performance. It is interesting to note that Fe_2P is not observed in the X-ray diffraction data, even when synchrotron radiation and high-resolution measurements are used. It indicates low and/or amorphous Fe_2P content in the sample and high sensitivity of the magnetic measurements to such ferromagnetic compounds. In summary, higher temperature, no matter the charge compensation mechanism, reduces the vanadium solubility limit by ejection of the supervalent ion from the olivine structure leading to formation of a NASICON phase and of other compounds. The existence of a NASICON phase has been reported for other dopant elements by many researchers at low dopant level for a synthesis temperature ≥650 °C.[11,22,23]

The observed dependence of the vanadium solubility on the synthesis temperature provides a base to analyze the available results on the vanadium substitution. Figure 10 compares unit cell volumes obtained in this work with those reported earlier. Most of the previous synthesis attempts were done at 650 or 700 °C. Hong's,[9] Hua's[10] and Ma's[11] results are consistent with each other and with our results, demonstrating nearly linear cell volume decrease up to 5% vanadium substitution at 700 °C[9,10] and up to 7% at 650 °C.[11] For higher vanadium contents, the data at 650−700 °C either terminates or the cell volume shows saturation, indicating that no more vanadium can be substituted. At 550 °C, the linear dependence extends up to 10% vanadium substitution, the result first obtained in this work.

This consistency also suggests the same vanadium oxidation state in these works, which according to our current findings, should be 3+. V^{4+} reported by Ma et al. is probably an artifact caused by using X-ray photoelectron spectroscopy, a surface technique, in contrast to bulk X-ray absorption used in this work. The cell parameters in our previous report[9] on V doping at P site are consistent with those obtained here and by others substituting the Fe site. Combining this with the fact that we could not reproduce substitution at P site in this work and with questionable stability of Fe^{2+} in the presence of V^{5+},[24] we conclude that vanadium was in fact substituted at the Fe site in that work.[9]

In cases when cell volume dependence on the vanadium concentration is ascending,[12] irregular,[13] or nonlinear[17] (Figure 10), the cell volume of unsubstituted $LiFePO_4$ is often also abnormal, either too high,[12,13] or too low.[17] This is indicative of structural defects, such as antisite disorder, typically observed at lower synthesis temperature,[7] or substitution at the Li site.[7,25] When the Li/Fe/V/P precursor ratio is not tailored for proper charge compensation, minor differences in the synthesis conditions might

dx.doi.org/10.1021/cm2017032 |*Chem. Mater.* 2011, 23, 4733–4740

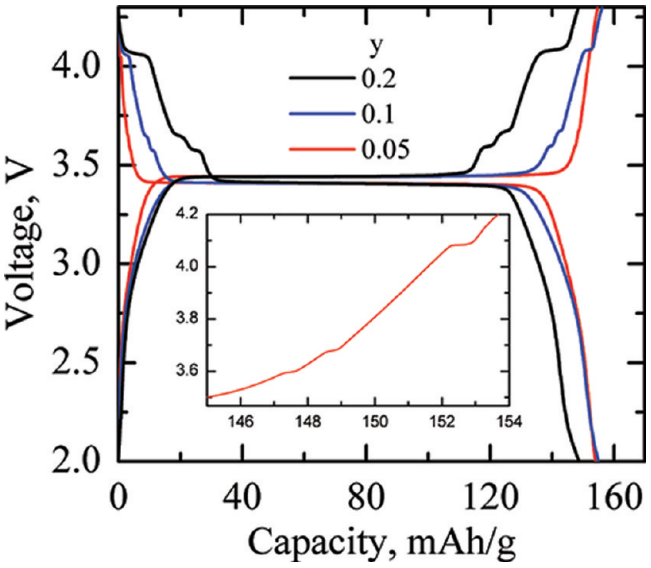

Figure 12. Galvanostatic charge−discharge curves measured at 0.1*C* (0.07 mA/cm^2) for $LiFe_{1-3/2y}V_yPO_4$ (y = 0.05, 0.1, 0.2) 700 °C samples. The inset shows the magnified region, Li removal, for the 5 mol % sample.

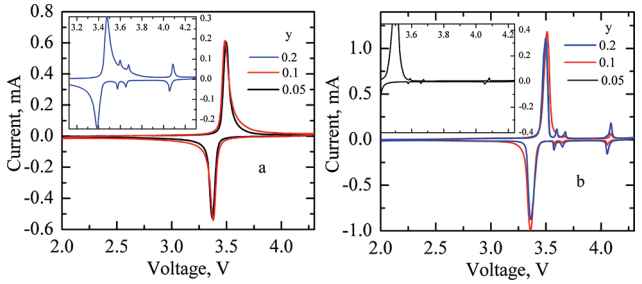

Figure 13. CV curves for $LiFe_{1-3y/2}V_yPO_4$ synthesized (a) at 550 °C and (b) 700 °C. The inset in part (a) shows the CV curve for the 20 mol % V synthesized at 550 °C, and the inset in part (b) shows the magnified region for the small redox peaks in 5 mol % of vanadium synthesized at 700 °C.

drive the system toward either Li or Fe or simultaneous Li and Fe-site substitution and vacancies formation at either site, resulting in irregular variation of the cell parameters.

The galvanostatic charge−discharge curves for selected vanadium substituted $LiFePO_4$ samples synthesized at 550 °C are shown in Figure 11. A single flat plateau at about 3.45 V is observed for up to 10 mol % vanadium substitution. With an increase in the vanadium concentration to 20 mol %, three additional redox plateaus are observed at 3.58, 3.68, and 4.1 V on charge. These plateaus correspond to those observed in $Li_3V_2(PO_4)_3$ during cycling. This data is in agreement with our XRD data that indicated the formation of a crystalline NASICON phase at 550 °C for the 20 mol % vanadium concentration. The 5 and 10 mol % vanadium compounds deliver a capacity of about 156 mAh/g. However, at 20 mol % vanadium substitution, the capacity drops to around 140 mAh/g. The 700 °C samples show extra redox plateaus for all levels of vanadium substitution, 5, 10, and 20 mol %, with the plateaus becoming more evident with the increase in the vanadium content (Figure 12). These plateaus are similar to that observed for the 20 mol % vanadium substituted sample prepared at 550 °C.

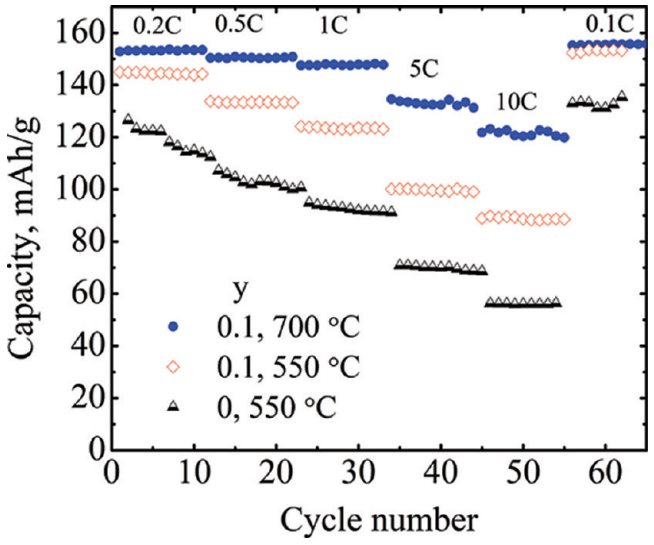

Figure 14. Cycling performances of $LiFe_{1-3y/2}V_yPO_4$ measured from a 0.1 to 10*C* rate, within a 2.0−4.3 V voltage window.

The cyclic voltammograms for the different compounds are shown in Figure 13. It is observed that compound synthesized at 550 °C with vanadium concentration ≤10 mol % shows a single redox peak similar to the pristine $LiFePO_4$. With an increase in the vanadium concentration to 20 mol %, three additional reversible redox peaks are observed. The 700 °C samples on the other hand show these additional peaks even at 5 mol % vanadium concentration (Figure 13b, inset). The intensity of these peaks increases with the increase in vanadium content (Figure 13b). The three additional redox peaks observed at 3.58, 3.68, and 4.1 V are associated with the redox potentials of $Li_3V_2(PO_4)_3$ for the first two lithium ion extractions $Li_3V_2(PO_4)_3$, $Li_{2.5}V_2(PO_4)_3$, $Li_2V_2(PO_4)_3$ to $LiV_2(PO_4)_3$, respectively.

Figure 14 shows the kinetics of reaction for selected samples. At 0.1*C* (~0.07 mA/cm^2), the pristine $LiFePO_4$ synthesized at 550 °C shows a capacity of 134 mAh/g, while at higher discharge current densities the sample delivers about 60 mAh/g. On the other hand, the 10 mol % V compounds, whether formed at 550 or 700 °C, show equal discharge capacities at 0.1*C* of 156 mAh/g; with an increase of the *C*-rate to 0.2*C*, a small difference is observed. This difference becomes larger with the increase in discharge rate and reaches 30 mAh/g at 10*C*. The enhanced electrochemical performance of the 10 mol % V-substituted sample synthesized at 550 °C is most likely to be the effect of substitution, since no sign of impurities were observed in high-resolution XRD, magnetic susceptibility, and CV curves.

The higher capacity and rate capability for the 700 °C materials could be due to the presence of the electrochemically active $Li_3V_2(PO_4)_3$ and/or to the presence of the electronically conductive Fe_2P impurities. At this time, we cannot differentiate between these two effects.

CONCLUSIONS

We have shown that at least 10 mol % of V^{3+} can be substituted at the iron site of $LiFePO_4$ at 550 °C forming a $LiFe_{1-3/2y}V_yPO_4$ solid solution, as confirmed by the linear change in lattice parameters with vanadium substitution. Vacancies on the iron site are formed to compensate for the V^{3+} charge. Increasing the synthesis temperature to 700 °C leads to decreased vanadium

dx.doi.org/10.1021/cm2017032 |*Chem. Mater.* 2011, 23, 4733–4740

solubility and formation of a $Li_3V_2(PO_4)_3$ phase. The electrochemical performance is improved by vanadium substitution possibly due to a reduction in the nucleation energy for the formation of the $FePO_4$ phase. However, the multiphase materials synthesized at 700 °C and containing $LiFe_{1-3/2y}V_yPO_4$, $Li_3V_2(PO_4)_3$, and Fe_2P show even better electrochemistry, probably because of the electronically conductive Fe_2P phase and the electrochemically active NASICON phase contributes to the electrochemical capacity. This critical impact of synthesis temperature on vanadium solubility explains the contradictory reports in the literature concerning the incorporation of vanadium into the olivine lattice.

AUTHOR INFORMATION

Corresponding Author

*Phone: (607) 777-4623. Fax: (607) 777-4623. E-mail: stanwhit@gmail.com.

ACKNOWLEDGMENT

This research is supported as part of the Northeastern Center for Chemical Energy Storage, an Energy Frontier Research Center funded by the U.S. Department of Energy, Office of Science, and Office of Basic Energy Sciences under Award Number DE-SC0001294. Use of the Advanced Photon Source at Argonne National Laboratory and National Synchrotron Light Source at Brookhaven National Laboratory is supported by the U.S. Department of Energy, Office of Science, Office of Basic Energy Sciences, under Contracts No. DE-AC02-06CH11357 and DE-AC02-98CH10886, respectively. We thank Dr. Bruce Ravel for the help with X-ray absorption data acquisition.

REFERENCES

(1) Padhi, A. K.; Nanjundaswamy, K. S.; Goodenough, J. B. *J. Electrochem. Soc.* **1997**, *144*, 1188.
(2) Yamada, A.; Chung, S. C.; Hinokuma, K. *J. Electrochem. Soc.* **2001**, *148*, A224.
(3) Huang, H.; Yin, S. C.; Nazar, L. F. *Electrochem. Solid State Lett.* **2001**, *4*, A170.
(4) Ravet, N.; Chouinard, Y.; Magnan, J. F.; Besner, S.; Gauthier, M.; Armand, M. *J. Power Sources* **2001**, *97*−*8*, 503.
(5) Chung, S. Y.; Bloking, J. T.; Chiang, Y. M. *Nat. Mater.* **2002**, *1*, 123.
(6) Herle, P. S.; Ellis, B.; Coombs, N.; Nazar, L. F. *Nat. Mater.* **2004**, *3*, 147.
(7) Chen, J. J.; Vacchio, M. J.; Wang, S. J.; Chernova, N.; Zavalij, P. Y.; Whittingham, M. S. *Solid State Ionics* **2008**, *178*, 1676.
(8) Islam, M. S.; Driscoll, D. J.; Fisher, C. A. J.; Slater, P. R. *Chem. Mater.* **2005**, *17*, 5085.
(9) Hong, J.; Wang, C. S.; Chen, X.; Upreti, S.; Whittingham, M. S. *Electrochem. Solid State Lett.* **2009**, *12*, A33.
(10) Hua, N.; Wang, C.; Kang, X.; Wumair, T.; Han, Y. *J. Alloys Compd.* **2010**, *503*, 204.
(11) Ma, J.; Li, B.; Du, H.; Xu, C.; Kang, F. *J. Electrochem. Soc.* **2011**, *158*, A26.
(12) Sun, C. S.; Zhou, Z.; Xu, Z. G.; Wang, D. G.; Wei, J. P.; Bian, X. K.; Yan, J. *J. Power Sources* **2009**, *193*, 841.
(13) Zhang, L.-L.; Liang, G.; Ignatov, A.; Croft, M. C.; Xiong, X.-Q.; Hung, I.-M.; Huang, Y.-H.; Hu, X.-L.; Zhang, W.-X.; Peng, Y.-L. *J. Phys. Chem. C* **2011**, *115*, 13520.
(14) Jin, Y.; Yang, C. P.; Rui, X. H.; Cheng, T.; Chen, C. H. *J. Power Sourses* **2011**, *196*, 5623.
(15) LFP-NCO Cathode Material. http://www.aleees.com/en/product/LFP-NCO.htm.
(16) Zhao, T.; Xu, W.; Ye, Q.; Cheng, J.; Zhao, H. F.; Wu, Z. Y.; Xia, D. G.; Chu, W. S. *J. Synchrotron Radiat.* **2010**, *17*, 584.
(17) Harrison, K. L.; Manthiram, A. *Inorg. Chem.* **2011**, *50*, 3613.
(18) Toby, B. H. *J. Appl. Crystallogr.* **2001**, *34*, 210.
(19) Larson, A. C.; VonDreele, R. B. *General Structure Analysis System (GSAS)*, Los Alamos National Laboratory Report LAUR 86-748, 2004.
(20) Ravel, B.; Newville, M. *J. Synchrotron Radiat.* **2005**, *12*, 537.
(21) Chernova, N. A.; Nolis, G. M.; Omenya, F. O.; Zhou, H.; Li, Z.; Whittingham, M. S. *J. Mater. Chem.* **2011**, *21*, 9865.
(22) Ellis, B.; Herle, P. S.; Rho, Y. H.; Nazar, L. F.; Dunlap, R.; Perry, L. K.; Ryan, D. H. *Faraday Discuss.* **2007**, *134*, 119.
(23) Meethong, N.; Kao, Y. H.; Speakman, S. A.; Chiang, Y. M. *Adv. Funct. Mater.* **2009**, *19*, 1060.
(24) Clemens, O.; Bauer, M.; Haberkorn, R.; Beck, H. P. *Z. Anorg. Allg. Chem.* **2011**, *637*, 1036.
(25) Wagemaker, M.; Ellis, B. L.; Lutzenkirchen-Hecht, D.; Mulder, F. M.; Nazar, L. F. *Chem. Mater.* **2008**, *20*, 6313.